Electrochimica Acta 53 (2008) 5934–5940

Contents lists available at ScienceDirect

Electrochimica Acta

journal homepage: www.elsevier.com/locate/electacta

The effect of Fe^{3+} on magnetic moment of electrodeposited CoFe alloys—Experimental study and analytical model

Stanko R. Brankovic*, Sang-Eun Bae, Dmitri Litvinov

Electrical and Computer Engineering Department & Center for Nanomagnetic Systems, University of Houston, Houston, TX 77204-4005, United States

ARTICLE INFO

Article history:
Received 25 January 2008
Accepted 26 March 2008
Available online 7 April 2008

Keywords:
Electrodeposition
Magnetic materials
CoFe films
Incorporation
Nucleation

ABSTRACT

The effect of Fe^{3+} concentration on saturation magnetic flux density (B_s) of electrodeposited $Co_{40-44}Fe_{60-56}$ films was investigated. The results show that if the conditions at the electrochemical interface for nucleation/precipitation of iron(III) hydroxide ($Fe(OH)_3$) are reached, the B_s of electrodeposited $Co_{40-44}Fe_{60-56}$ films quickly decreases as a result of the $Fe(OH)_3$ incorporation into deposit. These conditions are discussed as a function of the solution formulation (pH) and the parameters of electrodeposition process (current density, current efficiency, diffusion layer thickness) and a simple analytical model is developed qualitatively describing the hydroxide incorporation phenomenon and resulting decrease in B_s of $Co_{40-44}Fe_{60-56}$ films.

Published by Elsevier Ltd.

1. Introduction

The development of electrodeposited soft high magnetic moment (SHMM) alloys for magnetic recording applications has gone through several phases in the last three decades. In the beginning, the alloy of choice was $Ni_{81}Fe_{19}$ (Permalloy) with saturation magnetic flux density, $B_s = 1$ [T] [1]. The later development was followed by $Ni_{45}Fe_{55}$ alloys with 60% higher B_s values [2], and ternary CoFeNi alloys with lower Ni content and B_s ranging between 1.6 [T] and 2.2 [T] [3–7]. In recent years, the electrodeposited CoFe alloys with the highest possible magnetic moment of ≈2.4 [T] were demonstrated as well [6,8,9]. These alloys represent the most probable materials for fabrication of the future magnetic recording heads and, for this reason, the formulation and understanding of the experimental conditions for their deposition are the topics of research efforts in industry and academia as well.

One of the specifics of the ferromagnetic metals and alloys electrodeposition is that the hydrogen co-deposition occurs in parallel with the metal deposition process. Because of that, the current efficiency, γ, is lower than 1 and depletion of the hydrogen ions at the electrode/solution interface occurs leading to local increase in pH. This effect promotes formation of insoluble $M_x(OH)_y$ species at the electrode/solution interface and this is attributed as the main reason for incorporation of oxygen and nonmagnetic inclusions in Permalloy [10], CoFeNi [3] and in 2.4 [T] CoFe alloys [6,11]. The incorporation of metal hydroxides into deposit inevitably results in dilution of the saturation magnetic flux density of electrodeposited films. In the case of electrodeposited CoFe alloys, the incorporation of $Fe(OH)_3$ is the main obstacle for obtaining deposits with B_s equivalent to metallurgical CoFe alloys with same composition [8,9]. The presence of Fe^{3+} and $Fe(OH)_3$ in the plating solutions is mainly due to dissolved oxygen from air which oxidizes Fe^{2+} ions into Fe^{3+} ($O_2 + 4Fe^{2+} + 4H^+ \rightarrow 4Fe^{3+} + 2H_2O$). If the concentrations of Fe^{3+} and OH^- at the solution/electrode interface are such that the product of solubility for $Fe(OH)_3$ is exceeded, the hydroxide precipitation and incorporation into growing CoFe deposit occurs.

In this paper, the work investigating the effect of Fe^{3+} ion concentration on the decrease of saturation magnetic flux density of electrodeposited $Co_{40-44}Fe_{60-56}$ films is presented. The conditions leading to $Fe(OH)_3$ nucleation and precipitation at the electrode/solution interface are fully considered and the analytical model describing hydroxide incorporation into $Co_{40-44}Fe_{60-56}$ deposit is developed. The practical implications of this model for electrodeposition of high moment magnetic alloys are discussed.

2. Experimental

A standard three electrode cell configuration with solution volume of 5 L was used to electrodeposit 0.6 ± 0.05 μm thick $Co_{40-44}Fe_{60-56}$ films. The composition of electrodeposited films was chosen to be in the range ≈40 at.% Co and ≈60 at.% Fe so that the corresponding saturation magnetization of ≈2.4 [T] is expected

* Corresponding author at: Electrical and Computer Engineering Department, University of Houston, N308, Engineering Building 1, Houston, TX 77204-4005, United States. Tel.: +1 713 743 4409; fax: +1 713 743 4444.
E-mail address: Stanko.Brankovic@mail.uh.edu (S.R. Brankovic).

0013-4686/$ – see front matter. Published by Elsevier Ltd.
doi:10.1016/j.electacta.2008.03.071

Table 1
Solution design and parameters of the electrodeposition process

Solution components (mol L^{-1})	
$FeSO_4$	0.1
$CoSO_4$	0.046
$(NH_4)_2SO_4$	0.3
H_3BO_3	0.4
$FeCl_3$	0.0008–0.00275
Saccharin	0.7×10^{-3}
Process parameters	
j	3.8 mA cm^{-2}
ω	300 rpm
γ	~0.12
pH	2.0
T	298 K
Galvanostatic control	

[12]. The cathode was rotating Cu disk (d = 1.7 cm) and Co plate was used as an anode confined in separate cell compartment. The Cu disks are electropolished to mirror finish prior to each deposition experiment. The details of the plating solution and parameters of the electrodeposition process are described in Table 1. In freshly prepared solutions, the Fe^{3+} ions are introduced by addition of the certain amount of $FeCl_3$. The Fe^{3+} content in the bulk solution was monitored before and after the deposition experiments using titration method [13] and no measurable changes were observed. The composition of the CoFe films was verified by energy dispersive X-ray spectroscopy (EDX) and secondary ion mass spectroscopy (SIMS) (oxygen content). The magnetic moment of CoFe films was measured by vibrating sample magnetometer (VSM). The reported B_s values represent the average of at least three samples (five measurements per sample) for each composition of the solution (Fe^{3+} content). The error bar associated with each point is calculated as standard deviation of all measurements for samples obtained from particular solution composition. The thickness of the CoFe films was determined from scanning electron microscopy (SEM) images of the focused ion beam (FIB) cross-sections, from charge stripping and AFM step height measurements. All fits of the experimental data were performed using the least-square method.

3. Results and analytical model

3.1. Experimental results

The results from our measurements of B_s for $Co_{40-44}Fe_{60-56}$ films deposited from solutions containing different concentrations of Fe^{3+} are shown in Fig. 1 (B_s vs. $C_\infty^{Fe^{3+}}$). The solutions with very low concentration of Fe^{3+}, $C_\infty^{Fe^{3+}} \leq 0.00134$ mol L^{-1}, are yielding the $Co_{40-44}Fe_{60-56}$ films with B_s values of ≈2.41 [T]. Since the same B_s values are also reported for metallurgical $Co_{40-44}Fe_{60-56}$ alloys [12], we can state that in this range of $C_\infty^{Fe^{3+}}$ there is no measurable effect of Fe^{3+} on magnetic moment of $Co_{40-44}Fe_{60-56}$ films. The additional increase in concentration of Fe^{3+} in the plating solution yields the $Co_{40-44}Fe_{60-56}$ deposits with lower B_s. For solutions with $C_\infty^{Fe^{3+}}$ between 0.00134 and 0.0014 mol L^{-1} the B_s values are slightly lower, decreasing from ≈2.41 [T] to ≈2.32 [T]. The saturation magnetic flux density of $Co_{40-44}Fe_{60-56}$ films is decreasing steeply as the $C_\infty^{Fe^{3+}}$ in plating solution is further increased. The solution with $C_\infty^{Fe^{3+}} = 0.0020$ mol L^{-1} yields the $Co_{40-44}Fe_{60-56}$ films which show ≈44% decrease in B_s (≈1.35 [T]). However, the increase of $C_\infty^{Fe^{3+}}$ above the 0.002 mol L^{-1} does not seem to contribute to the further decrease of the magnetic moment. The B_s decreases insignificantly as the $C_\infty^{Fe^{3+}}$ increases further from 0.002 mol L^{-1} to ≈0.00275 mol L^{-1}.

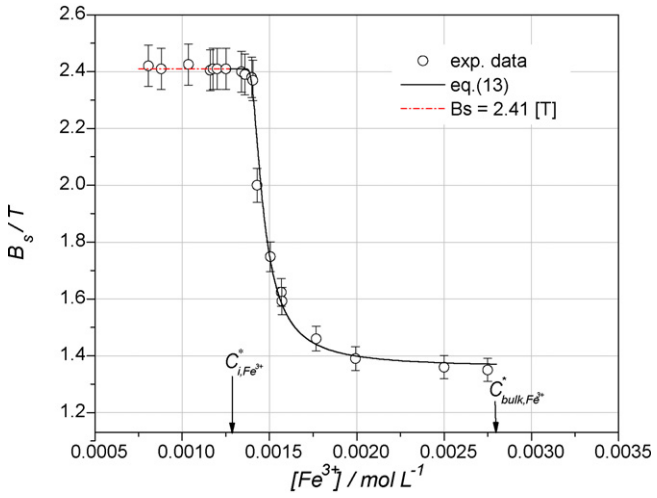

Fig. 1. The B_s values of the electrodeposited $Co_{40-44}Fe_{60-56}$ films from solutions with different concentrations of Fe^{3+}. The values of $C^*_{i,Fe^{3+}}$ and $C^*_{\infty,Fe^{3+}}$ are indicated by arrows. The black line represents the fit of Eq. (13). Dashed line (red) is B_s = 2.41 [T], see text for more details.

3.2. Solubility of iron(III) hydroxide—bulk solution

If the concentrations of the Fe^{3+} and OH^- in the bulk solution ($C_\infty^{Fe^{3+}}$, $C_\infty^{OH^-}$) are such that the product of solubility for $Fe(OH)_3$ is exceeded (K_p, Table 2 [14]) the precipitation of the hydroxide in the bulk solution is expected to occur. The necessary condition for precipitation of the $Fe(OH)_3$ from the bulk solution for known $C_\infty^{OH^-}$ can be expressed in terms of $C_\infty^{Fe^{3+}}$ as

$$C_\infty^{Fe^{3+}} > \frac{K_p}{(C_\infty^{OH^-})^3} \quad (1)$$

In the equation above, the concentration of OH^- ions in the bulk solution is the direct function of the concentration of H^+ ions through the ionic product of water [15]:

$$K_w = C_\infty^{H^+} \cdot C_\infty^{OH^-} \quad (2)$$

Substituting Eq. (2) into Eq. (1) and expressing $C_\infty^{H^+}$ as 10^{-pH} we can define the equilibrium or limiting concentration of Fe^{3+} in

Table 2
Numerical values of the constants and parameters used in the model

Parameter	Value	Unit	Reference
ν	0.01	$cm^2\ s^{-1}$	[18]
D_{H^+}	9.3×10^{-5}	$cm^2\ s^{-1}$	[17]
δ/D_{H^+}	$= 1.61 D_{H^+}^{-0.67} \omega^{-0.5} \nu^{0.17} = 66.4$	s cm^{-1}	Calculated
$D_{Fe^{3+}}$	0.55×10^{-5}	$cm^2\ s^{-1}$	[34]
$\delta/D_{Fe^{3+}}$	$= 1.61 D_{Fe^{3+}}^{-0.67} \omega^{-0.5} \nu^{0.17} = 439$	s cm^{-1}	Calculated
σ_{hyd}	0.1×10^{-4} to 0.2×10^{-4}	J cm^{-2}	[25]
$\rho_{m,Fe(OH)_3}$	0.031	mol cm^{-3}	[27]
$\upsilon_{m,Fe(OH)_3}$	$= \frac{1}{\rho_{m,Fe(OH)_3}} = 32.3$	$cm^3\ mol^{-1}$	Calculated
Ω	$\approx \frac{1}{\rho_{m,Fe(OH)_3} N_A} = 5.36 \times 10^{-23}$	cm^3	Calculated
$\rho_{m,Co,Fe}$	0.145	mol cm^{-3}	[33]
$\upsilon_{m,Co,Fe}$	6.90	$cm^3\ mol^{-1}$	Calculated
R_{CoFe}	$\approx \frac{\gamma j}{2F} = 2.36 \times 10^{-9}$	mol $cm^{-2}\ s^{-1}$	Calculated
k	1.38×10^{-23}	J K^{-1}	[28]
N_A	6.022×10^{23}	mol^{-1}	[28]
F	96,485	C mol^{-1}	[28]
K_p	2.79×10^{-39}	$mol^4\ L^{-4}$	[14]
K_w	1×10^{-14}	$mol^2\ L^{-2}$	[15]

the bulk, $C^*_{\infty,Fe^{3+}}$, for which the net precipitation or dissolution of hydroxide phase from or into the bulk solution are considered to be zero [9,16]:

$$C^*_{\infty,Fe^{3+}} = \frac{K_p}{(K_w)^3} \times 10^{-3\,pH} \quad (3)$$

3.3. Solubility of iron(III) hydroxide—solution/electrode interface

The net flux of hydrogen ions towards the electrode surface through the diffusion layer can be expressed as $J_{H^+} = j(1-\gamma)/F$, where j (deposition current) and γ (current efficiency) are the parameters of the deposition process (Table 1) and F is Faraday's constant (Table 2). By approximating the concentration gradient of hydrogen ions through the diffusion layer of thickness δ as linear function, $\partial C/\partial x = (C^{H^+}_\infty - C^{H^+}_i)/\delta$, the concentration of the hydrogen ions at the electrode/solution interface, $C^{H^+}_i$, can be estimated from the simple mass balance using the Fick's first law of diffusion:

$$\frac{j(1-\gamma)}{F} = (C^{H^+}_\infty - C^{H^+}_i) \cdot \frac{D_{H^+}}{\delta} \quad (4)$$

The ratio between hydrogen diffusivity in solution, D_{H^+}, and diffusion layer thickness, δ, can be evaluated using the data from literature [17] or it could be calculated if the kinematic viscosity of the solution is known [18] (Table 2). From Eq. (4), using the same procedure as in Section 3.2, the equilibrium concentration of the Fe^{3+} at the electrode/solution interface, $C^*_{i,Fe^{3+}}$, can be expressed combining Eqs. (2) and (1) applied for electrode/solution interface ($K_w = C^{H^+}_i \cdot C^{OH^-}_i$ and $C^{Fe^{3+}}_i = K_p/(C^{OH^-}_i)^3$). The final expression for $C^*_{i,Fe^{3+}}$ is then

$$C^*_{i,Fe^{3+}} = \frac{K_p}{(K_w)^3} \cdot \left(10^{-pH} - \frac{(1-\gamma)j}{F} \cdot \frac{\delta}{D_{H^+}}\right)^3 \quad (5)$$

The inspection of Eq. (5) and the fact that, $(1-\gamma)j/F\,(\delta/D_{H^+})$ is always >0, suggests that the conditions for $Fe(OH)_3$ precipitation at electrode/solution interface are reached for lower concentration of Fe^{3+} than for the bulk solution. The values of $C^*_{i,Fe^{3+}} = 0.00128\,mol\,L^{-1}$ (Eq. (5)) and $C^*_{\infty,Fe^{3+}} = 0.0028\,mol\,L^{-1}$ (Eq. (3)) are indicated in Fig. 1. As one can see, the magnetic moment of $Co_{40-44}Fe_{60-56}$ films starts to decrease for Fe^{3+} concentration that is $\approx C^*_{i,Fe^{3+}}$. This indicates that there is direct relationship between the decrease of B_s for $Co_{40-44}Fe_{60-56}$ films and necessary conditions for $Fe(OH)_3$ precipitation at the electrode/solution interface.

3.4. Heterogeneous nucleation of iron(III) hydroxide at electrode/solution interface

The driving force for nucleation of the $Fe(OH)_3$ from the solution is the difference between the chemical potentials of $Fe(OH)_3$ dissolved in solution and its counterpart in the crystalline (solid) phase ($\Delta\mu_{s/c}/RT = \Delta G_{s/c}/kT = \ln S$) [19]. This dependence is function of the term called saturation, S, and for the case of $Fe(OH)_3$ nucleation on the growing CoFe surface, the saturation term can be approximately defined as [19,20]:

$$S = \frac{C^{Fe^{3+}}_i}{C^*_{i,Fe^{3+}}}. \quad (6)$$

The term $C^{Fe^{3+}}_i$ represents the concentration of the Fe^{3+} ions at the electrode/solution interface and $C^*_{i,Fe^{3+}}$ is the equilibrium concentration of Fe^{3+} at electrode/solution interface defined by Eq. (5). The electrodeposition of $Co_{40-44}Fe_{60-56}$ films occurs at significantly more negative potential (≈ -1.19 V vs. SHE) than what is the equilibrium potential for Fe^{2+}/Fe^{3+} redox couple ($\Delta E^0_{Fe^{2+}/Fe^{3+}} = +0.771$ V vs. SHE [21]). Because of that, the certain depletion of Fe^{3+} at the interface is possible due to electrochemical reduction of Fe^{3+} to Fe^{2+} ($Fe^{3+} + e^- \rightarrow Fe^{2+}$) and due to $Fe(OH)_3$ incorporation into deposit. To accommodate this fact, we express $C^{Fe^{3+}}_i$ as a function of $C^{Fe^{3+}}_\infty$ by introducing the parameter p where $C^{Fe^{3+}}_i = pC^{Fe^{3+}}_\infty$ and p is such that $0 < p < 1$, implicating that $C^{Fe^{3+}}_i < C^{Fe^{3+}}_\infty$ is mathematically correct statement. We anticipate that consumption of the Fe^{3+} at the interface due to $Fe(OH)_3$ incorporation is significantly smaller than the consumption of the Fe^{3+} due to electroreduction process and because of that, the parameter p is considered to be constant, i.e. $p \neq f(C^{Fe^{3+}}_\infty)$. The more elaborate phenomenological description of parameter p is provided in Appendix B of this paper, and for now, we define the saturation S in terms of p, $C^{Fe^{3+}}_\infty$ and $C^*_{i,Fe^{3+}}$ as

$$S = \frac{pC_{\infty,Fe^{3+}}}{C^*_{i,Fe^{3+}}} \quad (7)$$

According to the classical nucleation theory, the nucleation rate J ($cm^{-2}\,s^{-1}$) of the crystals (solid) from the solution is the exponential function of the term which among other parameters includes the saturation [19,22,23]. For the case of $Fe(OH)_3$ nucleation on the growing CoFe surface the nucleation is considered to be heterogeneous. Assuming the hemispherical shape of nucleus, the nucleation rate, $J_{Fe(OH)_3}$, can be expressed as [22,23]:

$$J_{Fe(OH)_3} = \Xi \exp\left(-\frac{16\pi \cdot \sigma^3_{hyd}\Omega^2}{3k^3T^3 \cdot (\ln S)^2} \cdot \phi\right) \quad (8)$$

Here the terms σ_{hyd}, k and Ω represent the $Fe(OH)_3$ crystal/solution interfacial free energy ($J\,cm^{-2}$), Boltzman's constant ($J\,K^{-1}$) and the volume of the $Fe(OH)_3$ molecule (cm^3). The term Ξ is the nucleation rate constant ($cm^{-2}\,s^{-1}$) and for any practical consideration it is assumed to be independent on saturation [22]. The above expression is only valid for $S > 1$ (super saturation conditions) while for $S = 1$ the nucleation rate drops to zero. The values of $S < 1$ in the above expression have no physical meaning, since in this case, the under saturation conditions are established and no nucleation and growth of hydroxide phase is thermodynamically possible but rather its dissolution back into the solution. The term ϕ represents the shape factor which is defined in terms of the wetting angle, θ, between the $Co_{40-44}Fe_{60-56}$ film surface and newly formed hydroxide nucleus, $\phi = 0.25(2+\cos\theta)(1-\cos\theta)^2$ [24].

3.5. $Fe(OH)_3$ incorporation model

Since the growing $Co_{40-44}Fe_{60-56}$ surface represents the active morphology with great number of defects and preferable nucleation sites (steps, dislocations, grain boundaries, etc.), we expect that the average size of the stable $Fe(OH)_3$ nucleus is probably just a few molecules. We anticipate the scenario on the growing $Co_{40-44}Fe_{60-56}$ surface in which as soon as the stable nucleus of $Fe(OH)_3$ is formed, it immediately becomes an active nucleation center for arriving Co, or Fe adatoms, and it is instantaneously buried into deposit. In this situation, the controlling step of $Fe(OH)_3$ incorporation is the hydroxide nucleation itself. Assuming that steady state conditions apply, i.e. the hydroxide incorporation flux is equal to the flux achieved through the nucleation process, we define the $Fe(OH)_3$ incorporation rate in units of flux ($mol\,cm^{-2}\,s^{-1}$) as

$$R_{Fe(OH)_3} = \langle N_{Fe(OH)_3} \rangle \cdot J_{Fe(OH)_3} \quad (8)$$

In the above expression the $\langle N_{Fe(OH)_3}\rangle$ represents the average size of the stable nuclei (incorporated nuclei) in (mol) units and it can be further defined as an average number of molecules in stable nuclei, n_{molec}, divided by Avogadro's constant:

$$\langle N_{Fe(OH)_3}\rangle = n_{molec}/N_A. \quad (9)$$

Combining Eqs. (5)–(9) the final expression describing the $Fe(OH)_3$ incorporation rate into $Co_{40-44}Fe_{60-56}$ films is presented as

$$R_{Fe(OH)_3} = \frac{n_{molec}}{N_A}\cdot \Xi \exp\left(-\frac{16\pi\cdot\sigma_{hyd}^3\Omega^2}{3k^3T^3\cdot(\ln(pC_{\infty,Fe^{3+}}/(K_p/(K_w)^3\cdot(10^{-pH}-(1-\gamma)j/F\cdot(\delta/D_{H^+}))^3)))^2}\cdot\phi\right) \quad (10)$$

In the above expression, the only unknowns are the shape factor ϕ, the product $n_{molec}\Xi$, and the term p. The pH, δ, j, and γ are parameters related to the solution design and electrodeposition process and they are summarized in Table 1. The other terms in Eq. (10) are physical constants which are available in literature [14,15,25–28] or they could be calculated from the published data. They are summarized in Table 2.

4. Discussion

4.1. Model fit to the experimental results

The total volume of electrodeposited $Co_{40-44}Fe_{60-56}$ films used to calculate B_s in our measurements is obtained as the product of the film thickness and the geometrical area of the sample. If the electrodeposited film contains separate phases each having different magnetic moment and volume fraction in the film (α_i (%)), assuming that there is no mutual magnetic or electronic interactions influencing their magnetic moments, the measured B_s value of the film represent the volume average of the B_s values of the phases composing the film [29] $\left(B_{s,film} = \sum_{i=1}^{n}\alpha_i\cdot B_{s,i}\right)$. At room temperature, the $Fe(OH)_3$ can be considered as nonmagnetic, i.e. $B_{s,Fe(OH)_3} = 0$ [T] [30,31] and the dilution of the B_s of electrodeposited films due to $Fe(OH)_3$ incorporation can be simply modeled using the volume fraction of the nonmagnetic $Fe(OH)_3$ phase. In that sense, the measured saturation magnetic flux density of electrodeposited films ($B_{s,film}$) can be expressed as [32]:

$$B_{s,film} = B_{s,0}\cdot(1-\alpha_{Fe(OH)_3}) \quad (11)$$

The $B_{s,0}$ is taken to be 2.41 [T] and represents a value measured for the $Co_{40-44}Fe_{60-56}$ films electrodeposited from the solutions where no effect of Fe^{3+} is observed ($C_\infty^{Fe^{3+}} \le 0.00134\,mol\,L^{-1}$). The volume fraction of the $Fe(OH)_3$ in electrodeposited films can be calculated from the ratio between the $Fe(OH)_3$ incorporation rate expressed in ($cm\,s^{-1}$) units ($R_{Fe(OH)_3}\cdot\upsilon$), and the total film deposition rate expressed as $R_{film} = R_{Fe(OH)_3}\cdot\upsilon_{m,Fe(OH)_3} + R_{CoFe}\cdot\upsilon_{m,CoFe}$ ($cm\,s^{-1}$). In these expressions, $\upsilon_{m,Fe(OH)_3}$ and $\upsilon_{m,CoFe}$ represent the molar volume of $Fe(OH)_3$ and pure $Co_{40-44}Fe_{60-56}$ phase (Table 2). The $Fe(OH)_3$ volume fraction is then

$$\alpha_{Fe(OH)_3} = \frac{R_{Fe(OH)_3}\cdot\upsilon_{m,Fe(OH)_3}}{R_{CoFe}\cdot\upsilon_{m,CoFe} + R_{Fe(OH)_3}\cdot\upsilon_{m,Fe(OH)_3}}. \quad (12)$$

The deposition rate of $Co_{40-44}Fe_{60-56}$ phase, R_{CoFe}, is calculated from the parameters of the deposition process (Tables 1 and 2), while $\upsilon_{m,CoFe}$, and $\upsilon_{m,Fe(OH)_3}$ are constants available in the literature [27,33]. The $R_{CoFe}\cdot\upsilon_{m,CoFe}$ is calculated to be $1.63\times10^{-8}\,cm^{-2}\,s^{-1}$ (Table 2) while the value of $R_{Fe(OH)_3}$ is defined by Eq. (10) as the main result of our model. Combining Eqs (10)–(12), and using the values of the constants and parameters presented in Tables 1 and 2 we derive the complete analytical function that is used to fit the data presented in Fig. 1:

$$B_{s,film} = 2.41\,[T]\cdot\left(1-\frac{A\exp(-B\cdot(\ln(C\cdot C_\infty^{Fe^{3+}}))^{-2})}{1.63\times10^{-8}\,cm\,s^{-1}+A\exp(-B\cdot(\ln(C\cdot C_\infty^{Fe^{3+}}))^{-2})}\right). \quad (13)$$

The A, B, and C, are adjustable constants defined as

$$A = \frac{\upsilon_{m,Fe(OH)_3}\cdot n_{molec}\Xi}{N_A} = 5.36\times10^{-23}\ n_{molec}\Xi\ (cm\,s^{-1}) \quad (14)$$

$$B = \frac{16\pi\cdot\sigma_{hyd}^3\Omega^2}{3k^3T^3}\cdot\phi = 2.44\times10^3\,\phi\ [\emptyset] \quad (15)$$

$$C = \frac{p}{C_{i,Fe^{3+}}^*} = \frac{p}{0.00128}\ (mol^{-1}\,L) \quad (16)$$

The fit of Eq. (13) to the results in Fig. 1 for $C_\infty^{Fe^{3+}} \ge C_{i,Fe^{3+}}^*$ concentration range is shown with solid line (black). The values of the constants A, B, and C, from which the physical parameters $n_{nuc}\Xi$, ϕ and p are extracted, are summarized in Table 3. The dashed line (red online) in Fig. 1 represents the $B_{s,0} = 2.41$ [T], a value which is calculated as an average of the B_s measured for $Co_{40-44}Fe_{60-56}$ films obtained from solutions with $C_\infty^{Fe^{3+}} \le C_{i,Fe^{3+}}^*$. It is clear that the model described by Eqs. (10)–(16) succeeds in capturing the essential features of the experimentally observed dependence B_s vs. $C_\infty^{Fe^{3+}}$.

The extracted value of parameter p from the fit ($p = 0.96$) suggests that $C_i^{Fe^{3+}} \approx C_\infty^{Fe^{3+}}$ could be used as a valid approximation. In fact, a very good fit of the data in Fig. 1 is obtained using $p = 1$, and having only A and B as adjustable constants. We show the extracted parameters $(n_{nuc}\Xi)'$ and ϕ from this fit (Table 3), and they are very close to parameters $n_{nuc}\Xi$, and ϕ determined from the fit with Eq. (13). Having p value close to 1 indicates that the depletion of Fe^{3+} at the electrode/solution interface due to electroreduction of Fe^{3+} to Fe^{2+} and incorporation of $Fe(OH)_3$ is very small. Using the p, $n_{nuc}\Xi$, and ϕ (Table 3) we can evaluate how much of the Fe^{3+} depletion is due to the $Fe(OH)_3$ incorporation. As the limiting scenario, we use the maximum incorporation of $Fe(OH)_3$ into deposit as representative, which is calculated for $C_\infty^{Fe^{3+}} = 0.00275\,mol\,L^{-1}$ to be $3.8\times10^{-10}\,mol\,cm^{-2}\,s^{-1}$. Assuming that $R_{Fe(OH)_3} = J_{Fe^{3+}}$, for known $\delta/D_{Fe^{3+}}$ ratio (Table 2, [34]) we find that $C_i^{Fe^{3+}}/C_\infty^{Fe^{3+}}$ related to hydroxide incorporation is 0.99999983. Obviously, the contribution of the $Fe(OH)_3$ incorporation to Fe^{3+} depletion at the interface

Table 3
Numerical values of the fitting constants and corresponding estimate of the model parameters

Constant	Fit values	Estimated parameters
A	$(1.26\pm0.08)\times10^{-8}\,mol\,cm^{-2}\,s^{-1}$	$n_{molec}\Xi = 2.35\times10^{14}\,cm^{-2}\,s^{-1}$, Eq. (14)
B	0.012 ± 0.0046	$\phi\approx5.0\times10^{-6}$, $\theta\approx3^\circ$, Eq. (15)
C	$758\pm14\,mol^{-1}\,L$	$p = 0.96$, Eq. (16)
$A(p=1)$	$1.32\pm0.08\times10^{-8}\,mol\,cm^{-2}\,s^{-1}$	$(n_{molec}\Xi)' = 2.54\times10^{14}\,cm^{-2}\,s^{-1}$, Eq. (14)
$B(p=1)$	0.020 ± 0.0003	$\phi' = 8.2\times10^{-6}$, $\theta'\approx3.2^\circ$, Eq. (15)

is negligible. This implicates that our original assumption regarding the definition of p is correct and that most of the Fe^{3+} depletion is related to Fe^{3+} electroreduction. However, knowing that electrodeposition of $Co_{40-44}Fe_{60-56}$ films is conducted at ≈1.5 V more negative potential than the equilibrium potential of the Fe^{3+}/Fe^{2+} redox couple the difference between $C_i^{Fe^{3+}}$ and $C_\infty^{Fe^{3+}}$ of only 4% ($p = 0.96$) is still surprising. Perhaps the plausible explanation is that adsorbed additive on the CoFe surface (saccharin) hinders the electron transfer reactions such as Fe^{3+} reduction. Additional explanation could be that for the Fe^{3+} ions, being ~100 times less populated than Fe^{2+} and Co^{2+} in the bulk solution and at the electrode/solution interface, the probability of encountering the adsorption site which is energetically favorable for receiving an electron is very small. This results in slow kinetics of Fe^{3+} reduction.

The very small value of the shape factor ϕ and corresponding wetting angle θ obtained from the fit indicate a strong interaction between the CoFe surface and iron hydroxide. To some extent this is expected because the initial stage of Fe and Fe-like metal oxidation in aqueous environment typically starts with formation of 2D oxide/hydroxide films [35,36]. Although in our case, the driving force for hydroxide formation is not chemical or electrochemical nature, we expect that the interfacial free energy balance between the film, hydroxide and film/hydroxide interface which defines the wetting angle [24,24] is the same and the obtained value of θ has a valid physical meaning. The values of $n_{nuc}\Xi$ and $(n_{nuc}\Xi)'$ being in the range of 10^{14} cm^{-2} s^{-1}, is hard to compare with any data from the electrocrystallization literature since the most of the nucleation rate constants are measured for homogenous nucleation process. Their range has been reported to vary from 10^3 to 10^{20} [19,26]. In our case, assuming that the average size of stable nucleus is small ~100–1000 molecules, we calculate the values of Ξ to be in the range of 10^{11}–10^{12} cm^{-2} s^{-1}. However, at this point we cannot make any firm statement about the real value of Ξ. Future studies including HRTEM analysis of electrodeposited $Co_{40-44}Fe_{60-56}$ films are necessary in order to make reliable measurements of the size of incorporated hydroxide nuclei (n_{nuc}) and to estimate the real physical value of Ξ.

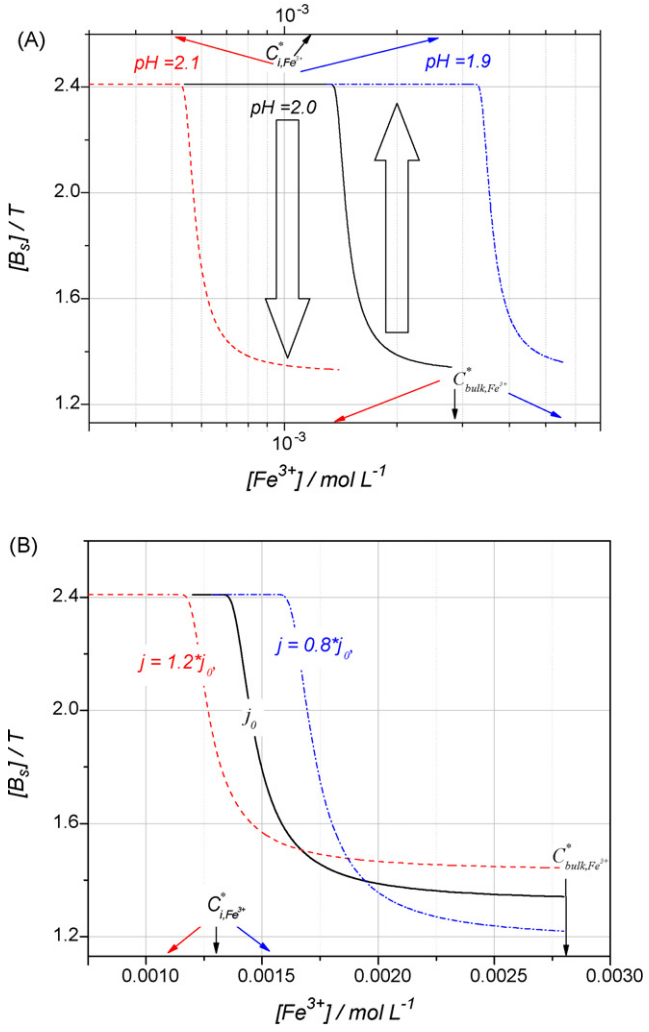

Fig. 2. (A) The effect of pH on B_s vs. $C_\infty^{Fe^{3+}}$ dependence. Curves are calculated using the same parameters except the pH. The arrows in the plot indicate the direction of the change of B_s due to increase or decrease of pH. (B) Calculated B_s. vs. $C_\infty^{Fe^{3+}}$ dependence for the films obtained form the same solution but with different current densities. The approximate values of $C^*_{i,Fe^{3+}}$ and $C^*_{\infty,Fe^{3+}}$ are indicated in both figures.

4.2. Effect of pH

It is helpful to use the values p, ϕ and $n_{nuc}\Xi$ (Table 3) to predict the effect of some crucial parameters of the electrodeposition process and solution design on resulting B_s vs. $C_\infty^{Fe^{3+}}$ dependence. In this exercise, we assume that p, ϕ and $n_{nuc}\Xi$ are *const* for small variations in solution pH or depositing current density. In Fig. 2A, the calculated B_s vs. $C_\infty^{Fe^{3+}}$ dependence for different pH of the solutions is presented as semi-log plot. The solution with pH = 2 is used as reference (black: bold). As it could be seen, for solution with $C_\infty^{Fe^{3+}} = 10^{-3}$ mol L^{-1}, which yields the $Co_{40-44}Fe_{60-56}$ films with B_s ≈2.41 [T], the increase in pH for less than 5% (from pH = 2 to 2.1, red: dashed line) would yield CoFe films with 40% lower B_s values (see the arrow). The same dependence but in opposite direction can be observed if the solution with $C_\infty^{Fe^{3+}} = 2 \times 10^{-3}$ mol L^{-1} and pH = 2 is considered. This solution yields $Co_{40-44}Fe_{60-56}$ films with $B_s \approx 1.4$ [T], however the situation can be greatly improved if the pH is lowered for 5% (from pH = 2 to 1.9). At pH = 1.9 it is still possible to comfortably produce 2.4 [T] $Co_{40-44}Fe_{60-56}$ films (blue: dash dot line). For any practical purpose it could be concluded that $Co_{40-44}Fe_{60-56}$ films with $B_s \approx 2.4$ [T] are produced from solutions that have $C_\infty^{Fe^{3+}}$ lower than $C^*_{i,Fe^{3+}}$ (Eq. (5), Fig. 2). The great sensitivity of B_s on pH for particular $C_\infty^{Fe^{3+}}$ is not surprising since the $C^*_{i,Fe^{3+}}$ is the exponential function of pH (Eq. (5)). The presented analysis brings the attention to the importance of the pH measurements accuracy and identifies the necessary level of pH control that ought to be established if the electrodeposition of high moment $Co_{40-44}Fe_{60-56}$ films is going to be considered for fabrication of future magnetic recording heads.

4.3. Effect of deposition current density

The magnetic structures that are produced today by through mask electrodeposition process are getting below the level of 100 nm in critical dimensions [9] and current crowding due to the secondary current distribution could have potentially large effect on their magnetic properties. Our model provides the opportunity to look some of these effects and to consider what kind of change in B_s vs. $C_\infty^{Fe^{3+}}$ dependence is produced if the small variations in current density occur. In Fig. 2B, using parameters from Table 3, the estimates of B_s vs. $C_\infty^{Fe^{3+}}$ dependence for three different current densities are presented. The value of $j_0 = 3.8$ mA cm^{-2} (Table 1) is taken as the referent one while the other deposition parameters are the same as in our experiments (black line: bold). The increase of current density of 20% ($j = 1.2j_0$, red: dashed line) results in shift of the $C^*_{i,Fe^{3+}}$ to ≈18% smaller value, i.e. the $Fe(OH)_3$ incorporation and the onset of B_s decrease start for 18% smaller $C_\infty^{Fe^{3+}}$. On the

other hand, the predicted value of B_s for $C_\infty^{Fe^{3+}} \rightarrow C^*_{\infty,Fe^{3+}}$ limit is ≈10% higher than in the case of j_0, (1.44 [T] for $1.2j_0$ vs. 1.34 [T] for j_0). The effect of 20% decrease in current density, $j = 0.8j_0$, is manifested through the shift of $C^*_{i,Fe^{3+}}$ to ≈20% higher value and in decrease of the lower limit of B_s for ≈9% (Fig. 2B, blue: dash-dot line). Obviously smaller deposition rates tolerate higher concentrations of Fe^{3+} at which 2.4 [T] $Co_{40-44}Fe_{60-56}$ films can be produced, but also result in larger volume fraction of incorporated $Fe(OH)_3$ once the value of $C^*_{i,Fe^{3+}}$ is significantly exceeded. The same conclusions should be applicable to the effect of diffusion layer thickness, and current efficiency as they are phenomenologically related to deposition rate, and in our model, they have the same functional relation to the rate of hydroxide incorporation (Eq. (10)). When electrodeposition of 2.4 [T] $Co_{40-44}Fe_{60-56}$ alloys in photoresist profiles with nanoscale dimensions is considered, the variation of local current density along the cross-section of the profile can not be avoided. We believe that presented considerations should be taken into account when designing the effective deposition conditions and solution chemistry to produce the nanostructures with desired magnetic moment.

5. Conclusion

The presented experimental results and analytical analysis (Eqs. (5), (10) and (13)) show that decrease of the saturation magnetic flux density of electrodeposited $Co_{40-44}Fe_{60-56}$ films is directly related to $Fe(OH)_3$ nucleation and precipitation at the electrode/solution interface. The concentration of Fe^{3+} at the interface, Eq. (5), for which the onset of hydroxide precipitation and incorporation into deposit starts was defined as a function of the bulk Fe^{3+} concentration and parameters of the electrodeposition process (j, γ, δ). The analytical model for hydroxide incorporation is developed (Eq. (10) and (13)) that qualitatively describes experimentally observed B_s vs. $C_\infty^{Fe^{3+}}$ dependence. The analysis of the model fit to experimental data suggests that depletion of Fe^{3+} at the interface due to the Fe^{3+} electroreduction and hydroxide incorporation is very small and that $C_i^{Fe^{3+}} \approx C_\infty^{Fe^{3+}}$ can be used as valid approximation. Our analysis shows that optimum conditions for electrodeposition of 2.4 [T] $Co_{40-44}Fe_{60-56}$ films are very sensitive to small changes in pH of the solution or magnitude of the deposition current density and that these consideration have to be taken into account with a great attention if the future high moment magnetic alloys and nanostructures for magnetic recording application are going to be produced by electrodeposition.

Acknowledgments

The authors would like to thank Dr. J. Rantschler for useful discussions regarding the B_s measurements. This work is sponsored by DOD, Strategic Environmental Research and Development Program, under contract # MM 1593 and by the 2007 GEAR program at University of Houston.

Appendix A. Nomenclature

$B_{s,film}$	saturation magnetic flux density of electrodeposited films
$B_{s,0}$	saturation magnetic flux density of $Co_{40-44}Fe_{60-56}$ phase
$C_{i,Fe^{3+}}$	concentration of Fe^{3+} ions at the electrode/solution interface
$C_\infty^{Fe^{3+}}$	bulk concentration of Fe^{3+} ions in the solution
$C_i^{H^+}$	concentration of H^+ ions at the electrode/solution interface
$C_\infty^{H^+}$	bulk concentration of H^+ ions in the solution
$C_i^{OH^-}$	concentration of OH^- ions at the electrode/solution interface
$C_\infty^{OH^-}$	bulk concentration of OH^- ions in the solution
$C^*_{i,Fe^{3+}}$	equilibrium concentration of Fe^{3+} ions at the electrode/solution interface
$C^*_{\infty,Fe^{3+}}$	equilibrium concentration of Fe^{3+} ions in bulk solution
D_{H^+}	H^+ ion diffusivity
$D_{Fe^{3+}}$	Fe^{3+} ion diffusivity
$J_{Fe^{3+}}$	flux of Fe^{3+} ions through the diffusion layer
$J_{Fe(OH)_3}$	nucleation rate of $Fe(OH)_3$
J_{H^+}	flux of H^+ ions through the diffusion layer
K_p	$Fe(OH)_3$ product of solubility
K_w	ionic product of water
n_{nuc}.	average size of the stable $Fe(OH)_3$ nucleus
R_{CoFe}	deposition rate of $Co_{40-44}Fe_{60-56}$ phase
$R_{Fe(OH)_3}$	incorporation rate of $Fe(OH)_3$ phase

Greek letters

$\alpha_{Fe(OH)_3}$	volume fraction of $Fe(OH)_3$ phase
δ	diffusion layer thickness
ϕ	shape factor
θ	wetting angle
$\rho_{m,Co,Fe}$	molar density of $Co_{40-44}Fe_{60-56}$ phase
$\rho_{m,Fe(OH)_3}$	molar density of $Fe(OH)_3$
σ_{hyd}	$Fe(OH)_3$/solution interfacial free energy
$\upsilon_{m,Fe(OH)_3}$	molar volume of $Fe(OH)_3$
$\upsilon_{m,Co,Fe}$	molar volume of $Co_{40-44}Fe_{60-56}$ phase
Ω	volume of $Fe(OH)_3$ molecule
Ξ	nucleation rate constant

Appendix B. Derivation of parameter *p*

At constant potential, the rate of Fe^{3+} electroreduction can be expressed as chemical reaction of the first order:

$$R_{Fe^{3+},ER} = k_{ER} \cdot C_{i,Fe^{3+}} \quad (A.1)$$

where k_{ER} is the rate constant dependent on potential of the electrode surface. The total rate of Fe^{3+} consumption at the electrode/solution interface (mol cm^{-2} s^{-1}) is equal to the sum of the rates of Fe^{3+} electroreduction and $Fe(OH)_3$ incorporation:

$$R_{Fe^{3+},T} = R_{Fe^{3+},ER} + R_{Fe(OH)_3} \quad (A.2)$$

The total rate of Fe^{3+} consumption, $R_{Fe^{3+},T}$, is equal to the flux of Fe^{3+} through the diffusion layer defined as

$$J_{Fe^{3+}} = \frac{D_{Fe^{3+}}}{\delta}(C_{\infty,Fe^{3+}} - C_{i,Fe^{3+}}) \quad (A.3)$$

Assuming that, for the range of investigated Fe^{3+} concentrations, $R_{Fe^{3+},ER} \gg R_{Fe(OH)_3}$ is valid approximation, combining Eqs. (A.1)–(A.3) we obtain

$$\frac{C_{i,Fe^{3+}}}{C_{\infty,Fe^{3+}}} \approx \frac{D_{Fe^{3+}}/\delta}{D_{Fe^{3+}}/\delta + k_{ER}} = p \quad (A.4)$$

References

[1] L.T. Romankiw, D.A. Thompson, US Patent 4,295,173 (1981).
[2] N. Robertson, H.L. Hu, C. Tsang, IEEE Trans. Magn. 33 (1997) 2818.
[3] I. Tabakovic, S. Remer, V. Inturi, P. Jalen, A. Thayer, J. Electrochem. Soc. 147 (2000) 219.
[4] T. Osaka, M. Takai, K. Hayashi, K. Ohashi, M. Saito, K. Yamada, Nature 392 (1998) 796.
[5] X. Liu, G. Zangari, M. Shamsuzzoha, J. Electrochem. Soc. 150 (2003) C159.
[6] E.I. Cooper, C. Bonhote, J. Heidmann, Y. Hsu, P. Kem, J.W. Lam, M. Ramasubramanian, N. Robertson, L.T. Romankiw, H. Xu, IBM J. Res. Dev. 49 (2005) 103.
[7] S.R. Brankovic, N. Vasiljevic, T. Klemmer, E.C. Johns, J. Electrochem. Soc. 152 (2005) C196.

[8] T. Osaka, T. Yokoshima, D. Shiga, K. Imai, K. Takashima, J. Electrochem. Soc. 6 (2005) C53.
[9] S.R. Brankovic, X.M. Yang, T.J. Klemmer, M. Siegler, IEEE Trans. Magn. 42 (2006) 132.
[10] S. Gadad, T.M. Harris, J. Electrochem. Soc. 145 (1998) 3699.
[11] T. Osaka, T. Yokoshima, D. Shinga, K. Imai, K. Takashima, Electrochem. Solid State Lett. 6 (2003) C53.
[12] R.M. Bozorth (Ed.), Ferromagnetism, IEEE Press, New York, 1978, p. 264.
[13] J.R. Roy, J.B. Thompson, Ind. Eng. Chem. 15 (1972) 747.
[14] D.R. Lide (Ed.), CRC Handbook of Chemistry and Physics, 86th edition, Tailor & Francis, Boca Raton, FL 2005, pp. 8–119.
[15] L. Pauling, College Chemistry, 3rd edition, W.H. Freeman, London, UK, 1964, p. 445.
[16] J.W. Mullin, Crystallization, 4th edition, Butterworth–Heinemann, Oxford, UK, 2001, p. 108.
[17] H. Schultz, M. Pritzker, J. Electrochem. Soc. 145 (1998) 2033.
[18] A.J. Bard, L. Faulkner, Electrochemical Methods Fundamentals and Application, vol. 1, 2nd edition, John Willey & Sons, New York, 2001, p. 339.
[19] J.W. Mullin, Crystallization, 4th edition, Butterworth–Heinemann, Oxford, UK, 2001, p. 128.
[20] The $Fe(OH)_3$ represents the sparingly soluble electrolyte which produces four ions, and the definition of saturation could have more elaborate forms than one presented. For simplicity reason, we use approximate definition expressed by Eq. (6) without jeopardizing the physical description of the nucleation process.
[21] A.J. Bard, L. Faulkner, Electrochemical Methods Fundamentals and Application, 2nd edition, John Willey & Sons, New York, 2001, p. 808.
[22] J.W. Mullin, Crystallization, 4th edition, Butterworth–Heinemann, Oxford, UK, 2001, p. 182.
[23] D. Kaschiev, Nucleation, Butterworth–Heinemann, Oxford, UK, 2000, p. 184.
[24] I.V. Markov, Crystal Growth for Beginners, World Scientific, New Jersey, 1995, p. 72.
[25] There are no reliable data in the literature for the value of $Fe(OH)_3$ crystal/solution interfacial free energy. Most of the literature data obtained from the nucleation measurements for sparingly soluble electrolytes fall within the range of 0.1×10^{-4} to 0.2×10^{-4} J cm^{-2}, and we take these values as representative, see Ref. [26].
[26] V.A. Gartem, R.B. Head, J. Chem. Soc. Faraday Trans. 1 (69) (1973) 514.
[27] D.W. Birch, A. Pring, A. Reller, H.W. Schmalle, Am. Miner. 78 (1993) 827.
[28] J.J. Tuma, Engineering Mathematics Handbook, 2nd edition, McGraw-Hill, New York, 1979.
[29] B.D. Cullity, Introduction to Magnetic Materials, Addison-Wesley Pub. Comp., London, UK, 1972, pp. 24, 152.
[30] C.A. McCammon, E. DeGrave, A. Pring, J. Magn. Matter 152 (1996) 33.
[31] E.N. Filho, E. Conforto, H.R. Rechenberg, J. Magn. Matter 74 (1988) 370.
[32] The use of Eq. (11) to model the dilution of B_s as a simple function of vol.% of incorporated $Fe(OH)_3$ is supported by the fact that this function predicts reasonably well the oxygen content in the CoFe films. For the films with 40% lower B_s (40 vol.% of $Fe(OH)_3$) using the molar volumes of CoFe and $Fe(OH)_3$ we calculate O at.% to be ≈4%. This is in a good agreement with our SIMS analysis ($O = 3 \pm 1$ at.%).
[33] S.R. Brankovic, R. Haislmaier, N. Vasiljevic, Electrochem. Solid State Lett. 10 (2007) D67.
[34] K.-M. Yin, J. Electrochem. Soc. 150 (2003) C435.
[35] M.R. Ryan, R.C. Newman, G.E. Thompson, J. Electrochem. Soc. 142 (1995) L177.
[36] R. Nishimura, Corrosion 43 (1987) 486.